MERCURY'S 2ND-DEGREE SHAPE AND GEOID: LUNAR COMPARISONS AND THERMAL ANOMALIES. Roger J. Phillips[1], Catherine L. Johnson[2,3], Mark E. Perry[4], Steven A. Hauck, II[5], Peter B. James[6], Erwan Mazarico[7], Frank G. Lemoine[8], Gregory Neumann[8], Stanton J. Peale[9], Matthew A. Siegler[10], David E. Smith[7], Sean C. Solomon[6,11], and Maria T. Zuber[7]. [1]Planetary Science Directorate, Southwest Research Institute, Boulder, CO 80302, USA (roger@boulder.swri.edu); [2]Department of Earth, Ocean and Atmospheric Sciences, University of British Columbia, BC, V6T 1Z4, Canada; [3]Planetary Science Institute, Tucson, AZ 85719, USA; [4]The Johns Hopkins University Applied Physics Laboratory, Laurel, MD 20723, USA; [5]Department of Earth, Environmental, and Planetary Sciences, Case Western Reserve University, Cleveland, OH 44106, USA; [6]Lamont-Doherty Earth Observatory, Columbia University, Palisades, NY 10964, USA. [7]Dept. of Earth, Atmospheric and Planetary Sciences, Massachusetts Institute of Technology, Cambridge MA 02139, USA; [8]NASA Goddard Space Flight Center, Greenbelt, MD 20771, USA; [9]Department of Physics, University of California, Santa Barbara, CA 93106, USA; [10]Jet Propulsion Laboratory, California Institute of Technology, Pasadena, CA, USA; [11]Department of Terrestrial Magnetism, Carnegie Institution of Washington, Washington, DC 20115, USA.

Introduction. Beyond a planet's first-order physical properties of radius, mass, and magnetic field are the properties of its geoid and shape ellipsoids (represented by spherical harmonic (SH) coefficients of degree $l = 2$ and order $m = 0$, 1 and 2). Such information constrains the radial density and rheological structures of the interior but may also may shed light on past mechanical, orbital, and spin states of the planet. Estimates of the 2nd-degree (l_2) geoid have been obtained from the radio science experiment on the MErcury Surface, Space ENvironment, GEochemistry, and Ranging (MESSENGER) spacecraft [1]. Reliable estimates of the low-degree shape coefficients are not possible with data from the Mercury Laser Altimeter (MLA), as the highly eccentric MESSENGER orbit precludes data acquisition in the southern hemisphere. A second source of absolute planetary radii determination is radio frequency observations that measure Mercury's radius at the time and location of occultations [2]. Occultation coverage in the southern hemisphere, combined with MLA data, support a spherical harmonic expansion of Mercury's shape to degree and order 8, with the l_2 estimate particularly reliable (Fig. 1).

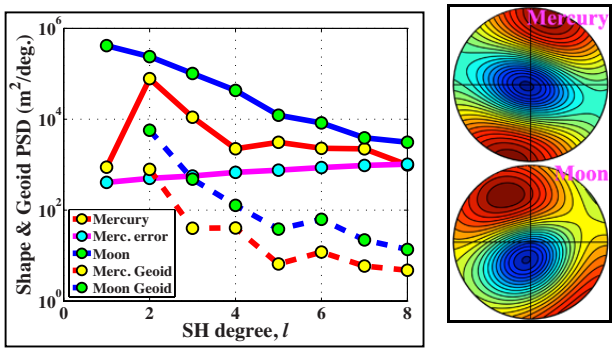

Figure 1. (Left) Power spectral densities (PSDs) for the Moon and Mercury. Solid lines are shape, dashed lines are geoid. (Right) Northern hemisphere views of Mercury and lunar shapes. For Mercury, the contour interval = 0.1 km, range ~ ±1 km; for the Moon, the contour interval = 0.2 km, range ~ ±2 km. 0° longitude is at bottom.

Here we compare Mercury's l_2 shape and geoid to their lunar counterparts. We consider reasons for the high correlation of Mercury's l_2 shape and geoid and propose a novel explanation based on Mercury's 3:2 spin-orbit resonance state.

Lunar comparisons. It has been long known that the lunar l_2 geoid is out of hydrostatic equilibrium [3,4] with respect to its current rotational and tidal potentials. Larger than equilibrium values (Table 1) of the gravity coefficients, C_{lm}, associated with polar flattening ($J_2 = -C_{20}$) and equatorial ellipticity (C_{22}) are described as "bulges," and there has been a debate for more than a century [5] as to whether or not these are rotational and tidal relics of an early Moon possessing a higher spin rate and smaller semi-major axis. It is a significant challenge to find valid mechanisms that might maintain these "fossil" bulges as the Moon spun down and moved away from the Earth [6–8]. Mercury's 2nd-degree spherical harmonic geoid coefficients are significantly farther from hydrostatic equilibrium than their lunar counterparts (Table 1, Fig. 1), a point evident [9] even from the poorly constrained coefficients estimated from the Mariner 10 flybys. Thus the innermost planet offers another opportunity to test the hypothesis that a large (i.e., gravity dominated) silicate-iron solar system body can preserve a record of its very early rotational and orbital history.

	Me	Mo
J_2(Obs)/J_2(Eql)	58	21
C_{22}(Obs)/C_{22}(Eql)	73	8
j_2(Obs)/j_2(Eql)	309	54
c_{22}(Obs)/c_{22}(Eql)	412	9

Table 1. Ratios of observed to upper-bound hydrostatic equilibrium values of l_2 geoid (J_2, C_{22}) and shape (j_2, c_{22}) coefficients of the Moon **(Mo)** and Mercury **(Me).**

The shape power spectral density (PSD) for Mercury indicates excess power in l_2 compared with other degrees (Fig. 1). The *z*- (short) axis of Mercury's l_2 shape ellipsoid is closely aligned with the planet's spin

axis (6° tilt vs. 27° for the Moon; Fig. 1), and the ellipsoid axes in the equatorial plane are only modestly misaligned from the principal axes (-15°; cf. 37° for Moon; Fig. 1). Mercury' l_2 shape and geoid have a high correlation coefficient (0.96 vs. 0.61 for Moon). Furthermore, a low admittance (0.1; see Fig. 1) implies that Mercury's l_2 shape is largely compensated. Mercury's l_2 shape coefficients are not only farther from equilibrium than their lunar shape counterparts, but they are also farther from equilibrium than Mercury's geoid. Given the high geoid/shape correlation and low admittance for l_2, along with the presence of a 3:2 spin-orbit resonance and its thermal consequences, the paths to the current states of hydrostatic disequilibrium may have been quite different for Mercury and the Moon.

Thermal anomalies and compensation models. Because of Mercury's 3:2 spin-orbit resonance, large orbital eccentricity (e), and near-zero obliquity, there are substantial temperature differences between the spin-axis poles (90° N/S) and the equator, and between 0°E/180°E and 90°E/270°E ("hot poles" and "cold poles," respectively) [10, 11]. Here we consider the hypothesis that parts of the l_2 shape and geoid can be explained by subsurface thermal density anomalies resulting from the propagation of these spatially varying surface temperatures into the interior. We note that l_2 accounts for ~95% of the spectral power of the surface temperature distribution. Capture of Mercury into a 3:2 resonance is nearly certain at e between 0.2 and 0.41 [12], and once captured the resonance is very stable [13]. The effects of chaotic variations in e [14], which mainly affect hot/cold pole temperature ratios, should likely be smoothed out in the subsurface. The temperature distribution will thus reflect the long-term mean value of e, close to the present value of 0.2056.

A simple test of the thermal hypothesis assumes one-dimensional conductive temperature profiles anchored at the surface by hot (434 K) and cold (329 K) pole temperatures [11] but isothermal at the core-mantle boundary. Converting temperature differences to density differences yields a geoid C_{22} close to the observed value, depending on the choice of linear thermal expansion coefficient, $\alpha_v/3$. To explore this idea further, we adopted an isostatic compensation model [15] to solve explicitly for crust-mantle boundary (Moho) relief (Airy compensation, δr_{20} or δr_{22}) and lateral density variations representing the thermal anomalies (Pratt compensation, $\delta\rho_{20}$ or $\delta\rho_{22}$). The two parameters varied in the solution space were mean crustal thickness, T_c, and the thermal layer thickness, M, extending from the surface to an assigned isothermal depth. Additional parameters were held constant (e.g., crust and mantle densities).

An example of the fraction of the c_{22} shape explained by the thermal layer is shown in Fig. 2. In this case the isothermal depth arbitrarily was set to 370 km, below which it is assumed that viscous flow has removed lateral density anomalies. The difference between hot and cold pole [11] conductive temperature profiles was converted to a thermal term ${}^T\delta\rho_{22}$ using $\alpha_v = 3\times10^{-5}$ K^{-1} and averaging over M. The magenta curves bound solutions satisfying the ${}^T\delta\rho_{22}$ constraint within ±3 kg /m^3. We prefer solutions with T_c < ~100 km [16], leading to a lower bound on M of ~300 km, a Moho relief of ~1 km, and thus nearly 100% of shape support by the thermal layer. We note that 2/3 of the thermal mass anomaly is within 150 km of the surface, and an entirely conductive thermal regime is a plausible state for present-day Mercury [17].

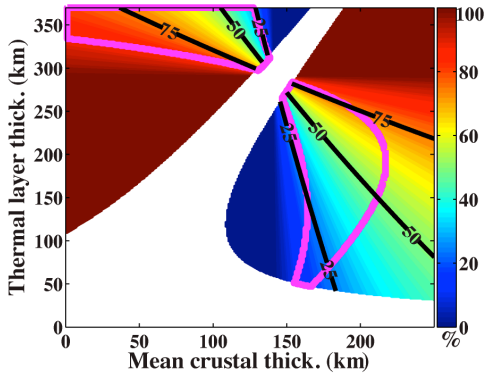

Figure 2. Fraction of c_{22} shape due to thermal anomalies (25%, 50%, 75% contours shown). Blank area contains physically implausible solutions. Color saturation at 100% (0%) indicates over-compensation by thermal layer (Moho relief). Magenta curves bound surface temperature constraint.

Conclusions. Mercury is remarkably far from hydrostatic equilibrium compared with the Moon. The axes of the surface thermal ellipsoid must align with the axes of the geoidal ellipsoid (principal moments), but there are no *a priori* requirements for the shape ellipsoid to do the same. Here we demonstrate the plausibility of one mechanism for support of Mercury's shape that takes advantage of the existing geoid-constrained thermal geometry.

References. [1] Smith D. E. et al. (2012) *Science*, *336*, 214-217. [2] Perry M. E. et al. (2011) *Planet. Space Sci., 59*, 1925-1931. [3] LaPlace P. S. (1798-1827) *Traité de Mécanique Céleste,* v. 2, bk 5, ch. 2. [4] Jeffreys H. (1970) *The Earth*, 5th ed., Cambridge Univ. Press. [5] Sedgwick W. F (1898) *Messenger Math., 27*, 171. [6] Garrick-Bethell I. et al. (2006) *Science*, *313*, 652. [7] Meyer J. et al. (2010) *Icarus, 208,* 1-10. [8] Matsuyama I. (2013) *Icarus*, *222,* 411-414. [9] Matsuyama I. and Nimmo F. (2009) *J. Geophys. Res.*, *114,* E010101. [10] Vasavada A. R. et al. (1999) *Icarus*, *141*, 179-193 [11] Siegler M. A. et al. (2013) *J. Geophys. Res. Planets*, *118,* 930-937. [12] Makarov V. V. (2012) *Astrophys. J.*, *752*, 73. [13] Noyelles B. et al. (2013) *DPS 45*, abstract 102.01. [14] Laskar, J. (1988) *Astron. Astrophys.*, *198*, 341–362. [15] Sleep N. H. and Phillips R. J. (1985) *J. Geophys. Res., 90, B6,* 4469-4489. [16] Smith D. E. et al. (2010) *Icarus, 209*, 88–100. [17] Michel N. C. et al. (2013) *J. Geophys. Res. Planets, 118,* 1033–1044.